PIV INVESTIGATION OF THE FLOW CHARACTERISTICS IN 2-LEG INTERNAL COOLANT PASSAGES OF GAS TURBINE AIRFOILS

D. Chanteloup, A. Bölcs

Laboratoire de Thermique appliquée et de Turbomachines (LTT)
Département Génie Mécanique (DGM)
Swiss Federal Institute of Technology (EPFL)
1015 Lausanne, Switzerland
denis.chanteloup@epfl.ch ; albin.boelcs@epfl.ch

ABSTRACT

A study of flow in a stationary model of a two-pass internal coolant passage is presented which focuses on the flow characteristics in the 180-deg bend region and downstream of the bend, where the flow is redeveloping. A stereoscopic digital PIV system measured all three velocity-components simultaneously to obtain mean-velocity and turbulence quantities of the flow field. The coolant passage model consisted of two square passages, each having a 20 hydraulic diameter length, separated by a web of 0.2 passage widths and connected by a sharp 180 deg bend with a rectangular outer wall. Ribs were mounted on the bottom and top walls of both legs with a staggered arrangement and at 45 deg to the flow. The rib height and spacing were 0.1 and 1.0 passage heights, respectively. The measurements were obtained for a flow condition with a Reynolds number of 50,000. The geometry is similar in the straight sections to a previous configuration but has ribs extending into the bend region. The paper presents new measurements of the flow in the straight legs of the passage, comparison of the flow in the bend region with a previous configuration and details of the flow recovery from the bend in the second leg.

NOMENCLATURE

x	Cartesian coordinate in axial duct direction
y	Cartesian coordinate in cross duct direction
z	Cartesian coordinate in horizontal duct direction
θ	Cylindrical coordinate in streamwise direction
r	Cylindrical coordinate in radial direction
U	Mean velocity component in x direction
V	Mean velocity component in y direction
W	Mean velocity component in z direction
U_θ	Mean velocity component in streamwise direction in bend
U_r	Mean velocity component in radial direction in bend
u'	Fluctuating velocity component in axial direction
v'	Fluctuating velocity component in cross duct direction
w'	Fluctuating velocity component in vertical direction
u'_θ	Fluctuating velocity component in streamwise direction
u'_r	Fluctuating velocity component in radial direction
U_b	Bulk mean-velocity
L	Test section length

D Height and width of passage legs, D=100 mm
D_h Hydraulic diameter D_h =D
B Thickness of divider plate
P Rib pitch
e Rib height
S Section length in bend at 90° section
k Turbulent kinetic energy $\frac{\frac{1}{2}\left(\left(u'^2+v'^2+w'^2\right)\right)}{U_b^2} \Leftrightarrow \frac{\frac{1}{2}\left(\left(u_\theta'^2+u_r'^2+v'^2\right)\right)}{U_b^2}$ *in bend*

INTRODUCTION

For the design of gas turbine blades, a detailed knowledge of the physical phenomena in the passage is necessary. Although CFD simulations can provide a better understanding of these phenomena, the numerical heat transfer predictions are not yet sufficiently accurate for design purposes. This is especially true for the complicated heat transfer patterns in the bend region of stationary or rotating coolant passages with rib-roughened walls. To improve the performance of the CFD codes, a validation of the predictions is necessary and detailed measurements of the flow structure in the passages are required for comparison.

In the present study, the particle-image-velocimetry (PIV) method was employed for the investigation of the flow field in a model of a stationary two-pass coolant passage. PIV was chosen for this study because it provides a high data acquisition rate and a good spatial resolution of the measured flow fields. The measurement with a single-camera PIV system of the highly three-dimensional flows in coolant channels and bends can contain substantial errors. The out-of-motion of the tracers (perpendicular to the light sheet plane) produces a systematic measurement error depending on the distance from the optical axis, e.g. [1]. In principle, an error correction for the in-plane components is feasible if the out-of-plane component of the flow is known. However, [2] applied the correction to single-camera 3D PIV velocity measurements and showed that the effect of the out-of-plane motion cannot be corrected completely, although the correction does improve the measurement accuracy. This measurement error can be avoided by using a stereoscopic PIV setup. [3] presented a comprehensive analysis of the translation method and an application to rotating disc flow. [4] reported on three-dimensional velocity measurements with an angular digital two-camera stereoscopic PIV system. A stereoscopic digital PIV system, based on the angular displacement method, was used for the present investigation. This PIV system is capable of simultaneously measuring all three velocity-components. Subsequently, an ensemble average of the velocity data in identical spatial windows is calculated to determine the mean and fluctuating velocity field.

This paper presents initial results from the Brite-Euram project for Internal Cooling of Turbine Blades (ICTB) measured with a PIV system. The velocity results presented are from the base configuration of four geometries to be investigated in this task. Heat transfer measurements will subsequently be performed with the same configurations. The specific objectives of the present paper are to determine the influence of the rib placement in the near bend regions on the flow fields upstream, inside and downstream of the bend and to provide new measurements of developed flow between ribs.

EXPERIMENTAL SETUP

Test Facility

A sketch of the test section is shown in Figure 1. Air was the working medium and was supplied by a continuously running compressor. Upstream of the test-rig, the mass flow is measured by means of a 5864S Brooks flow meter with a 1-percent accuracy. The air enters the settling chamber with an inner diameter of 600 mm via a 150-mm tube and a conical entrance section with an angle of 30 deg. The settling chamber is equipped with a combination of perforated plates, honeycombs and meshes to reduce unsteadiness and swirl in the flow.

Test section length	L	20 D_h
Height & Width of passage legs	D	1 D_h
Bend cross section	S	1 D_h
Length of divider plate		19 D_h
Thickness of divider plate	B	0.2 D_h
Rib cross-section		0.01D_h^2
Rib pitch	P	1 D_h
Rib height	e	0.1 D_h
Rib angle of attack		45deg

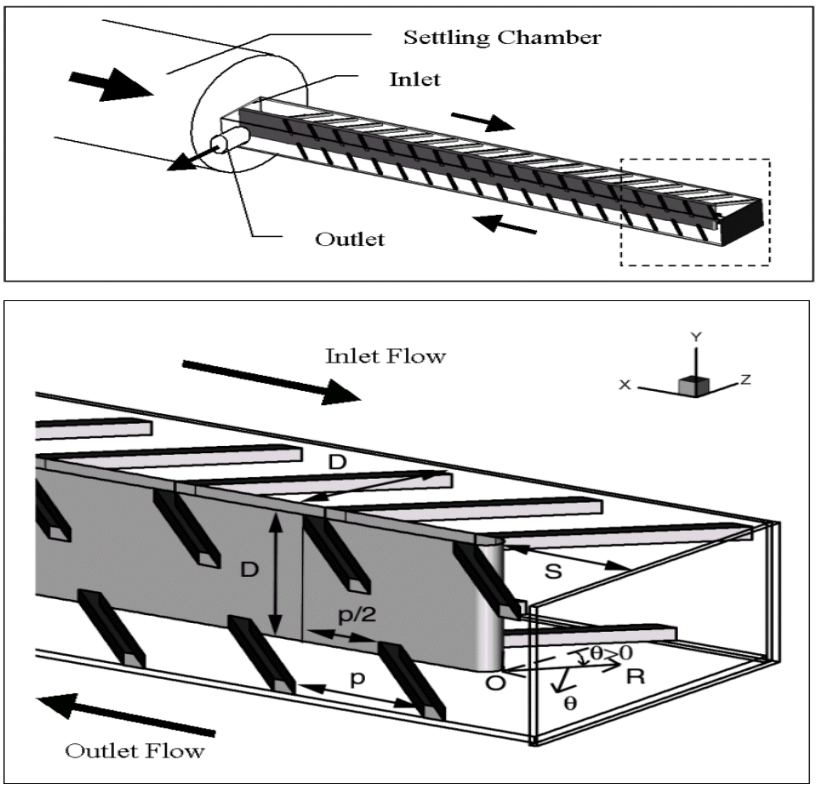

Figure 1 The internal coolant passage test facility and turn region details

A modular concept was chosen for the test section that allows an easy exchange of the components. The test section is a two-pass, cooling passage model of a gas turbine blade. The flow path in the downstream and upstream passages has a cross-section of 100*100mm^2 with a corresponding hydraulic diameter, $D_H = 100mm$, and a length of $20D_H$. The outer walls of the test section are made of 5-mm-thick extruded Plexiglas to obtain good optical properties for the PIV experiment. In the straight-corner bend, the clearance between the tip of the divider plate and the outer wall is equal to 1 D_h. The thickness of the divider plate or web between the two passages is $0.2D_H$. The tip of the divider plate is cylindrically shaped with a $0.1D_H$ radius. Square ribs with an angle of 45 deg to the passage centerline, rib heights of 0.1 hydraulic diameters ($e/D_H = 0.1$), and rib spacing of 10 rib heights ($P/e = 10$) are mounted in a staggered arrangement on the top and bottom wall of the passage. The ribs in the bend region and the dimensions of the bend are shown in Fig 2. Eighteen ribs are mounted on each of the top and bottom walls in each of the upstream and downstream passages of the model (18 * 4).

The total model test section including the test section entrance is turned 90 deg around the x-axis to obtain additional measurement planes without changing the flow conditions in the passage. This allows an easy optical access to the positions of interest for the PIV measurements.

Flow conditions, measurement program and coordinate systems

The measurements were obtained with air as working medium, at a flow Reynolds number of 50,000 (corresponding to a bulk velocity: $Ub = 7.58m/s$), at the entrance of the test section. The Reynolds number is based on the hydraulic diameter of 0.1 m with an air temperature of 20 C. The turbulence level is approximately 3 percent at the model inlet. An experimental study was conducted to assess the effect a varying test section orientation on the flow. The small variations between the flow conditions are within the measurement uncertainty and can therefore be neglected for the experiments.

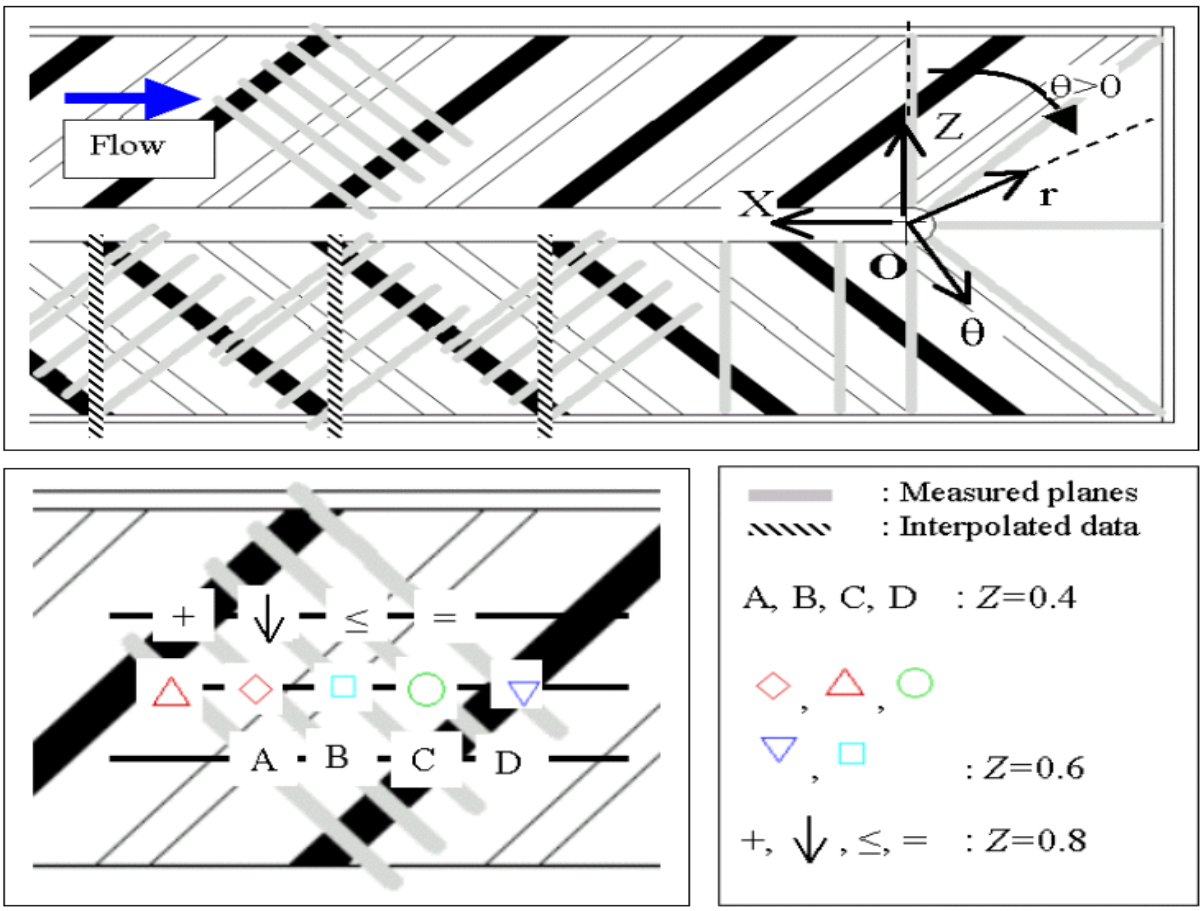

Figure 2: Measurement sections. The symbols represent the measurement lines (y direction) that will be analyzed in the next sections (Figure 3 and Figure 4).

Detailed measurements of the flow structure in the passage have been obtained in the bend, upstream ($3D_H$) and downstream ($4D_H$) of the 180 deg bend. The definition of the coordinate systems in the test facility is shown in Figure 2. A Cartesian coordinate system is used for the straight passages and a cylindrical coordinate system is used for the bend region. The origin for both coordinate systems is set on the bottom wall at the center of the rounded end of the divider plate for both coordinate systems. In the Cartesian (x, y, z) system, x is defined as positive in the streamwise direction of the flow downstream of the bend exit, y is defined positive vertically upwards in the horizontal test section orientation, and z is defined as shown. In the cylindrical (θ, r, y) coordinate system, the radial component r is defined as positive in the direction towards the outer wall, the streamwise component θ is defined as positive following the flow along the circular path centered on the center of the circular bend tip, and y is defined as for the Cartesian system.

PIV system

Di-Ethyl-Exyl-Sebacat (DEHS) from TOPAS is used as a tracer for the PIV experiments. This tracer appeared non-toxic, compared to olive oil or paraffin oil used in the past. A DLR-made Aerosol Generator using Laskin Nozzles generates 1-3 µm-diameter DEHS droplets. The droplets are injected upstream of the settling chamber to guarantee a homogeneous seeding density in the test section. The particles produce good light scattering in the 90° direction according to the Mie law.

A 1.5-mm thick light sheet that illuminates the particles is created by a Quantel Twins B Nd-Yag double oscillator pulsed laser. The laser provides light pulses having a maximum energy of 320mJ at a wavelength of 532 nm. The time delay between a pair of pulses can be

adjusted from 1μs to 1s with pulse duration of 5 ns. A plano-concave lens (-30 mm focal length) combined with two plano-cylindrical lenses (76.2 and 300 mm focal length) transform the beam into the vertical light sheet.

The imaging system consists of two independent Kodak ES1.0 cameras, each having its own PC. A Nikon Nikkor 55mm lens is mounted on each camera. The ES1.0 has a CCD interline transfer sensor with a pixel array of 1008(H) by 1018(V) pixels. Each pixel measures nine microns square with a 60 percent fill factor using a micro lens. The camera outputs 8 bit digital images with 256 gray levels. For a typical recording situation, the cameras are placed with an oblique angle of 4.3º at a distance of 0.7m from the light sheet plane. The pulse separation time is about 40 μs. The complete system, including laser, light sheet optics and camera, is mounted on a traversing system that allows an easy traverse to the position of interest.

The laser components (flash lamp and Q-switch) and the cameras are triggered by 10Hz TTL signals that are dispatched to all the elements with specific delays. As the different delays between both Flash lamps on the one hand, and between each Flash lamp and its Pockel cell on the other hand, are all different, they are generated by a programmable sequencer, the SEQUENCER Mod.919.4, made by the DLR Goettingen. The sequencer allows the generation of complex pulse patterns on multiple channels. The pulse width, the pulse interval, the number of pulses and the output channel number are freely programmable and their resolution is of 50 ns.

The frame grabber is an Imaging Technology PCI frame grabber with 2 MB memory onboard. The PCs are equipped with 384 MB RAM and 14 GB hard disk space. During the PIV measurement series, 10 images are written in real time into the PC's RAM memory. Subsequently, the acquisition is stopped and the images are saved on the hard disk. The automation of the process allows storing a maximum of 5000 frames per measurement plane.

Data Reduction

The 3D PIV measurements are obtained from the combination of two 2-dimensional vector fields; each of them measured from two different observation locations (the right and left cameras). The recordings from the right and left cameras are interrogated independently with the PIV software package VISIFLOW from AEA Technology. The cross-correlation analysis method is used with an interrogation window size of 64 by 64 pixels and 50 percent overlap between the interrogation windows. The frames provided by the cameras have a 992-pixel by 992-pixel resolution, which yield a 30 by 30 velocity-vector field per measurement plane. The raw data contains a small number of spurious vectors (<0.1 percent). The vector field is filtered with a predefined velocity magnitude threshold. Vectors that do not fall within the thresholds are removed and the remaining gaps are filled in with a weighted average of the surrounding vectors.

From the processed vector fields, the instantaneous three-dimensional velocity field can be reconstructed. Matlab homemade reconstruction software was developed at the EPFL-LTT. With angular PIV systems, where both cameras observe the light sheet from the same side, the corresponding interrogation positions in the right and left images do not match in general. Therefore, a calibration of the camera system is performed which also corrects for the distortion of the images in the lenses and the Plexiglas walls of the passage.

In addition to the mean-velocity field, the normal and shear stress quantities of the flow are required to evaluate numerical codes. In order to obtain PIV measurements in these forms, the statistical distribution of the velocity components is determined in identical spatial windows from a series of instantaneous PIV measurements. From these statistical distributions, the ensemble average and the statistical central moments are calculated to determine the desired mean-velocity field and Reynolds stresses.

Uncertainty analysis

[2], [5], [6] demonstrated the applicability of the presented stereoscopic PIV technique in details. Following are comments on small variations from those measurements (see also [7]).

For the present case, the mean number of particles per interrogation window (32 by 32 pixel^2) was set to 30. The average in-plane displacement of the particles is approximately 6 pixels, which is less than $0.25D_I$ in each direction, D_I being the characteristic dimension of the interrogation window. The optimal light sheet position for PIV measurement has the beam waist in the middle of the measurement section that provides a constant light sheet thickness in the measurement section. In the present investigation, the light sheet energy is so intense in the beam waist that the model Plexiglas walls are burned by the light sheet. The beam waist is placed outside of the section, which leads to a 10 percent variation of the light sheet thickness (mean thickness ≈ 1.2 mm) inside the section. An experimental study showed that the results are not significantly affected by the variation.

The estimation of the uncertainty of stereoscopic PIV velocity measurements requires the consideration of several aspects. Systematic errors occur due to the uncertainty in the determination of the geometrical parameter and the fabrication tolerances of the camera devices and lenses. Non-systematic errors are mainly due to the uncertainty in the determination of the average particle displacement in the interrogation region. The errors depend on the size of the interrogation region, the time separation between the laser pulses, the magnification of the recording, the out-of-plane velocity component, the turbulence of the flow, the length scale of the flow etc. The choice of the recording and interrogation parameters is therefore of significant importance for accurate and reliable velocity measurements. Using the method of [8], the mean value of the measured velocities is calculated by taking the instantaneous velocity measurements of the sample, summing the values, and dividing by the number of samples:

$$\bar{x} = \frac{1}{N}\sum_{i=1}^{N} x_i \tag{1}$$

In a similar manner, a measure of the fluctuating velocities can be obtained from the sample variance:

$$s^2 = \frac{1}{N-1}\sum_{i=1}^{N} (x_i - \bar{x})^2 \tag{2}$$

In the equations x and s^2 are the *sample mean* and *sample variance*, respectively. The number of observations N used to compute the estimates is called the *sample size*. Using the method of [8] The uncertainty for the mean velocity values of the present measurements is of order of 1 percent with a confidence level of 95 percent. The uncertainty of the mean velocity depends on the normal stresses and as a consequence is higher in regions where the turbulence level is high. The uncertainty level of the normal stresses of the Reynolds tensor, with a confidence level of 95 percent, is 8 percent of the normal stress values. The uncertainty of the normal stresses depends only on the number of samples and on the confidence level. Further details of the uncertainty method are given in [6].

RESULTS AND DISCUSSION

The objectives of the present paper are to determine the influence of the rib placement in the near bend regions on the flow fields upstream, inside and downstream of the bend and to provide new measurements of developed flow between ribs. Following are data and discussion on these topics.

Flow in the upstream leg

A comparison of velocity components in the developed flow region of a similar coolant passage was presented by [9]. The measurements showed that the flow with a 45-deg rib arrangement differs from the flow in a similar passage with a 90-deg rib arrangement [10]. With 90 deg ribs, a developed flow condition in terms of mean velocity and turbulent kinetic energy was achieved after 3 rib modules. The flow in the passage with 45° rib arrangement

requires a longer development length; at least 8 rib modules are needed to achieve a developed flow condition for the mean velocity components and 12 rib modules are required for the turbulent kinetic energy of the flow. In the present configuration, 18 rib-modules are placed in the upstream leg, to produce a developed flow field before the 180-deg bend.

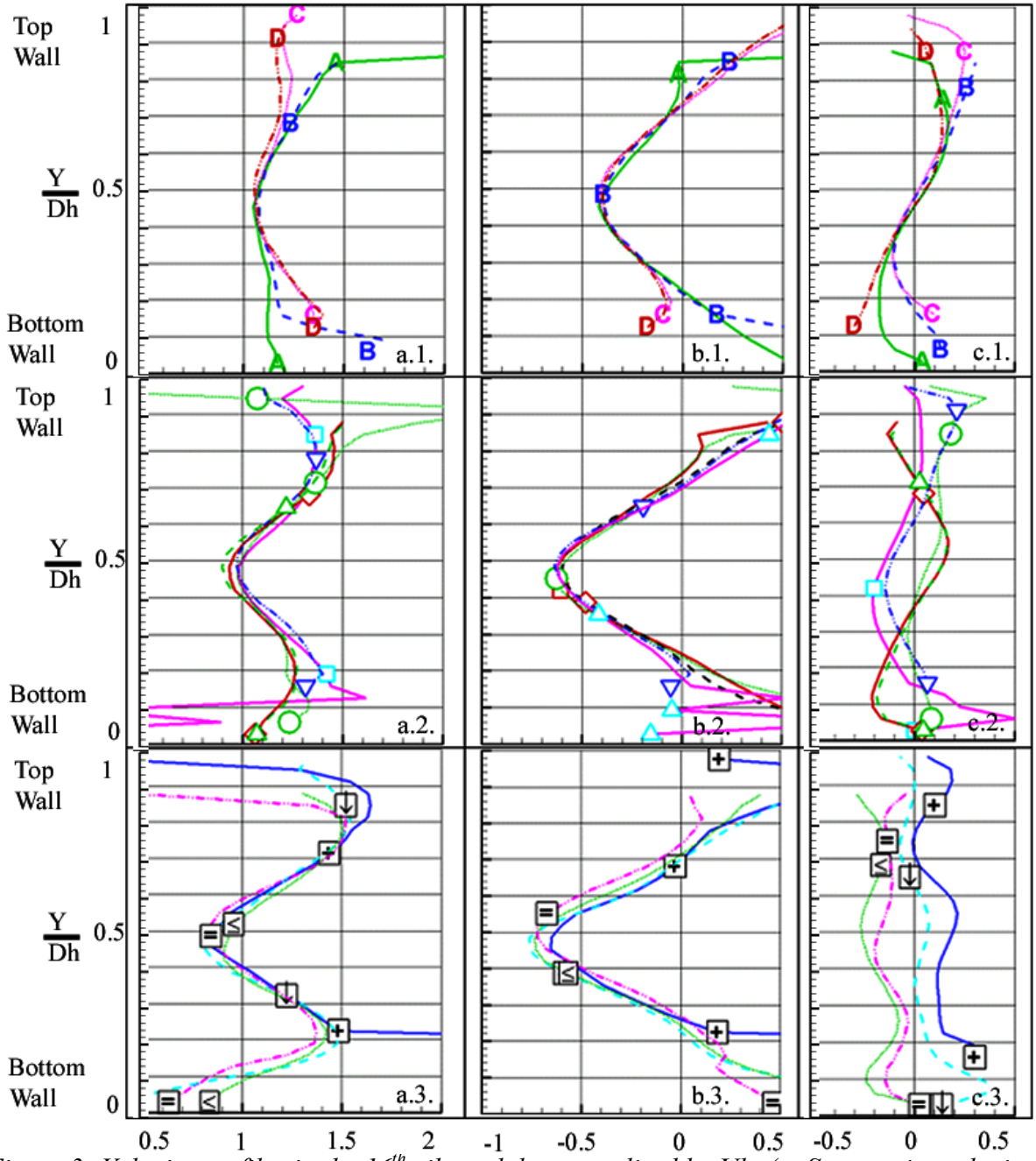

Figure 3: Velocity profiles in the 16th rib module, normalized by Ub. (a: Streamwise velocity, U; b: Velocity along Z-axis, W; c: Vertical velocity along Y-axis, V; 1: $Z=0.4D_H$; 2:$Z=0.6D_H$; 3:$Z=0.8D_H$). See Figure 2 for exact locations in the rib module.

The velocity components downstream of the 16th rib module are judged to be in a developed flow region. The streamwise (U), cross-stream (W) and normal (V) velocity profiles at selected streamwise and cross-stream locations are shown in Figure 3. The streamwise locations are between $X = 2.1$ and 3.1 (All the distances are normalized by D_H). The cross-stream locations are at $Z = 0.4$, 0.6 and 0.8. Note that the web wall location is at

$Z = 0.1$. Data from values of $Y = 0.06$ to 0.94 are plotted except at the rib surfaces where the closest value of has a $\Delta Y = 0.06$. The measurement procedures with this PIV set of optics has a probe dimension of $\Delta Y = 0.06$. At values of Y closer than 0.06 to the wall, spurious results were obtained due to wall light reflections.

As noted by [9], the streamwise velocity profiles have two peaks at values of Y approximately equal 0.2 and 0.8. These are attributed to the acceleration of the flow as it crosses the ribs at $Y = 0.1$ and 0.9 for the top and bottom walls, respectively. In the region near the downstream wall, $X = 0.8$, the velocity profiles are close to a single shape. The velocity at the centerline is near 0.9. The two peaks in the rib region are between 1.3 and 1.6. The flow at the centerline of the passage, $X = 0.6$ and $Y = 0.5$, also has a streamwise velocity of approximately 0.9. The streamwise velocities in the peak regions vary from 1.25 to 1.6 or more. This large variation is attributed to measurement locations close to the ribs, e.g., $X = 2.63$. The stream wise velocities at $Z = 0.4$, have a common minimum of $U = 1.07$. The velocity profiles nearer the walls vary depending upon streamwise location.

The cross-stream velocity profiles show a well-behaved increase in velocity as the fluid moves from the web or upstream wall to the outer or downstream wall. The peak velocities of 0.4 at $Z = 0.4$ increase to 0.65 at $Z = 0.8$.

The velocities normal to the ribbed walls have a more complex shape, which reflects the secondary flow pattern caused by the ribs. The velocity directions near the walls, e.g., $Y = 0.1$ and 0.9 are compatible with the single large secondary flow cell.

The turbulent kinetic energy profiles for the measurement locations of Figure 3 are shown in Figure 4. The profiles are complex but explainable in terms of the velocity profiles and proximity to the wall. For all three spanwise locations, the minimum value of k is about 0.025. A local minimum occurs near $Y = 0.5$ where the velocity gradients are low. Local maximum values occur in the high shear regions in the central part of the passage and near the walls.

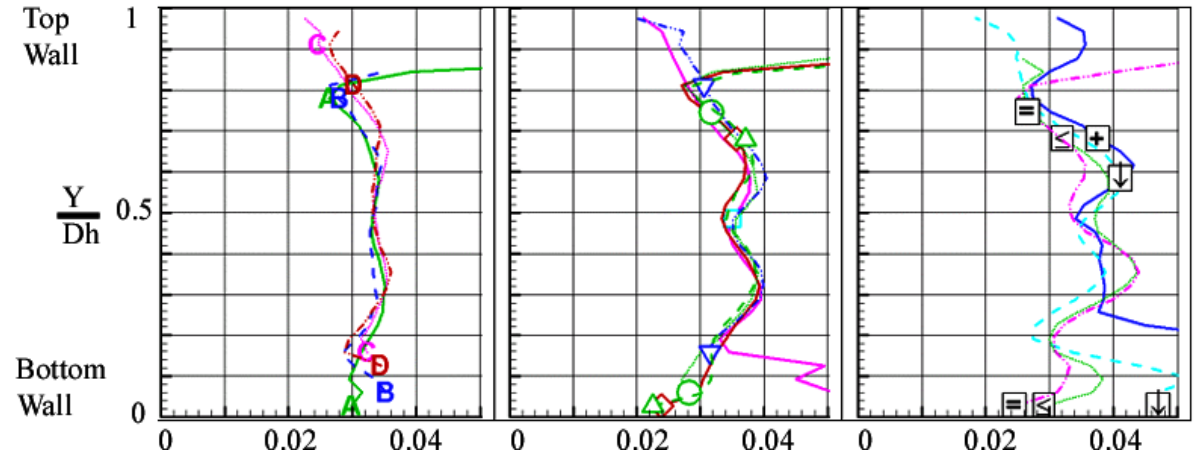

Figure 4: d: Turbulence kinetic energy in the 16th rib module (k / Ub^2). 1: Z=0.4Dh; 2:Z=0.6Dh; 3:Z=0.8Dh). E.g. Figure 2 for exact locations in the rib module.

These results provide a set of measurements that can be used to evaluate codes and turbulent transport models in the developed flow region of a ribbed channel. This flow in this region is as "periodic" as will probably be obtained in most coolant channels. The data provides a good test for codes to predict flow and heat transfer with various turbulence models and wall approximations.

Flow in the bend region

The flow in the bend region is more complex than in the ribbed region. The flow in the bend starts with the secondary structure from the ribs at $\theta = 0$ deg. Analysis of 100 PIV data sets at $\theta = 0$, 45, 90 135 and 180 deg in the bend showed that the secondary flow or vortex

structure has the vortex core at different locations in the instantaneous flow fields. The variation in core location appears to increase as the flow progresses through the bend. This variation appears to be unsteadiness in the flow. In the data reduction process, the unsteadiness is calculated as an increased turbulence fluctuation. Thus numerical simulation of the flow may require unsteady flow calculations rather than Reynolds-stress turbulence modeling.

Mean streamwise velocity contours and secondary flow vectors obtained at $\theta = 0$, 45, 90, 135 and 180 deg in the bend are presented in Figure 5. As noted before, these average velocity results were obtained from 1250 full-field data sets. For this set of results, the orientation of the view is always into the oncoming flow with the web at the left-hand side of the figure.

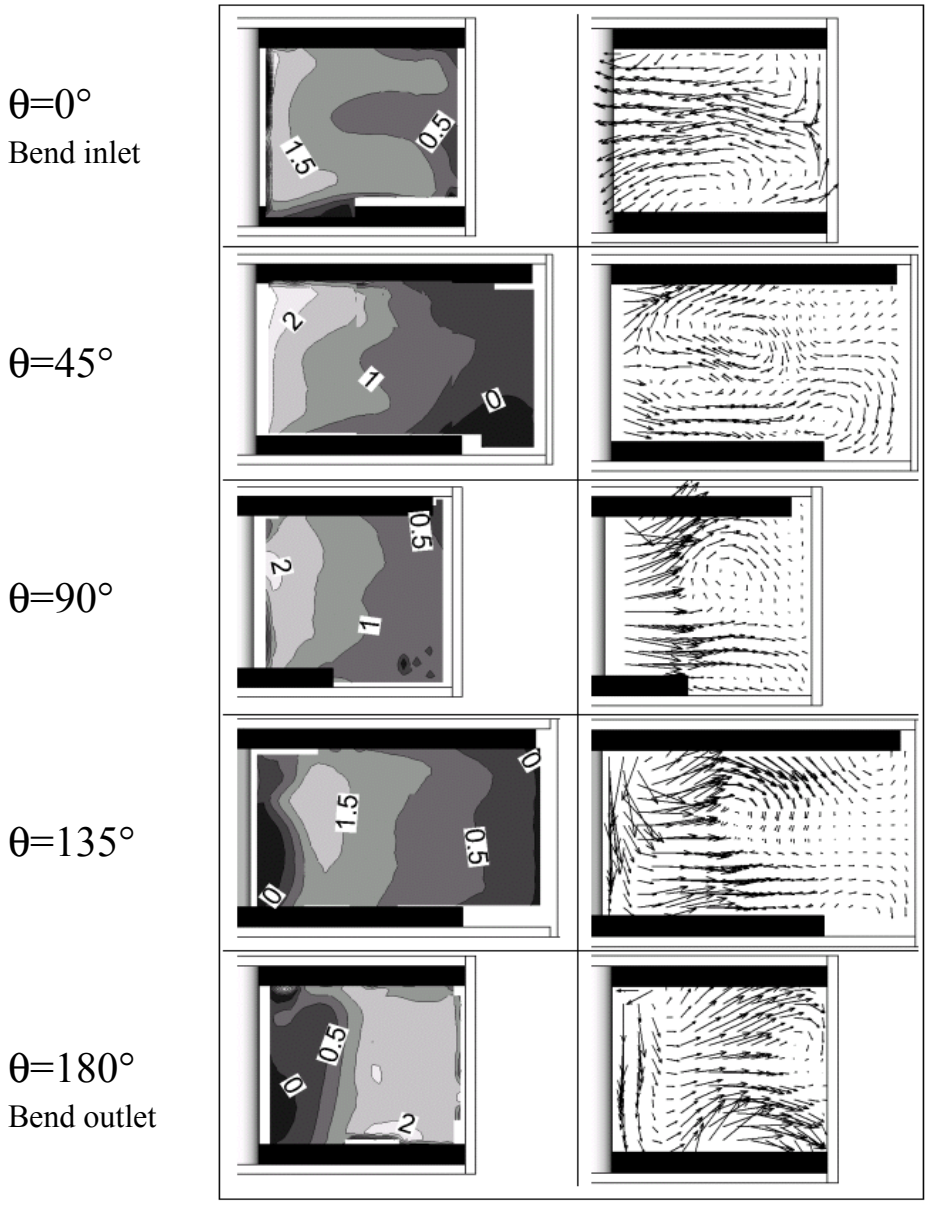

Figure 5: Mean streamwise velocity contours and secondary flow vectors obtained at θ=0, 45, 90, 135 and 180 deg in the bend. The contour lines values, U_θ, are plotted on the figures (U_θ / Ub).

At $\theta = 0\,\text{deg}$, the streamwise velocity distribution and the secondary flow patterns in the center region show the effects of the bend (Figure 3). However the secondary flow near the top and bottom wall that is connected with the rib orientation has decreased from that shown in Figure 3 for the developed flow between ribs. The streamwise flow near the inner web has begun to accelerate, indicating that this flow has entered the bend region. Note that near the web, all the secondary flow vectors are toward the web.

At $\theta = 45\,\text{deg}$, the streamwise velocity increases to more than 2 near the inner web and has a small region of negative velocities in the lower outside corner region. This negative velocity region is smaller than measured by [10]. The decreased recirculation cell size is attributed to the extension of the ribs into a portion of the bend region. The high streamwise velocity near the inner web is compatible with the conservation of angular momentum in the bend region. Note that near the web, the secondary flow vectors are away from the web.

At $\theta = 90\,\text{deg}$, the streamwise velocities of the flow have decreased near the web. The size of the region near the web where the secondary flow is away from the web has increased. The upper secondary cell seen at 45 deg continues but the lower cell has disappeared.

At $\theta = 135\,\text{deg}$, the flow has separated from the web and the streamwise velocities are negative. The average position of the vortex cell has moved toward the web and the secondary flow is generally away from the web. The streamwise velocity has a negative value near the outer wall, indicating a small recirculation cell.

At $\theta = 180\,\text{deg}$, a small region of recirculation occurs near the web and the lower wall. The upper rib, which extends into the bend region, has influenced the flow near the upper wall and probably decreased recirculation in that region. Note that the highest streamwise velocities have moved from near the web to the outer half of the passage and are 1.5 to 2.0 times the bulk velocity.

The conclusion from these data and from comparison with previous results [10] is that the combination of the rounded web and the ribs extending into the bend region has caused a decrease in the recirculation cells near the web and the outside corners of the bend. The unsteady character of the flow may require time dependent numerical techniques to accurately simulate the flow. The area near the web is likely to have large variations in heat transfer due to the high variations in streamwise velocity and may produce hot and cold spots and possibly increased stresses with their thermal gradients.

Flow in the downstream leg

Downstream of the bend is another region with relatively large variations in heat transfer. The streamwise velocity contours immediately downstream of the bend, $0.0 < X < 4.0$, at four heights are presented in Figure 6. The secondary flow vectors from the same region are presented in Figure 7.

The streamwise velocity contours at $Y = 0.89$ for $0.0 < X < 1$ are markedly different from those at the same heights for $1.0 < X < 4.0$. The streamwise velocity in the regions around the ribs appears to readjust to rib dominated flow in less distance than the flow in the center portion of the coolant passage, $Y = 0.3$, 0.5, and 0.7. The flow at $X = 4.0$ has not reached the same streamwise velocity distribution as measured for the developed flow region of the upstream leg.

The secondary flow vectors show the flow characteristics in the flow reattachment and adjustment region. In the center region of the passage there is a stronger flow toward the web than for the developed flow region as the streamwise velocities are being redistributed from their high values at the $X = 0$ or $\theta = 180\,\text{deg}$ toward the developed flow values shown in Figure 3.

The recirculation zone downstream of the bend disappears before $X = 0.1$. The reattachment length and extension of the recirculation cell into the passage is less for this model than that of [10]. The heat transfer distribution downstream of $X = 1.0$ is expected to be relatively periodic.

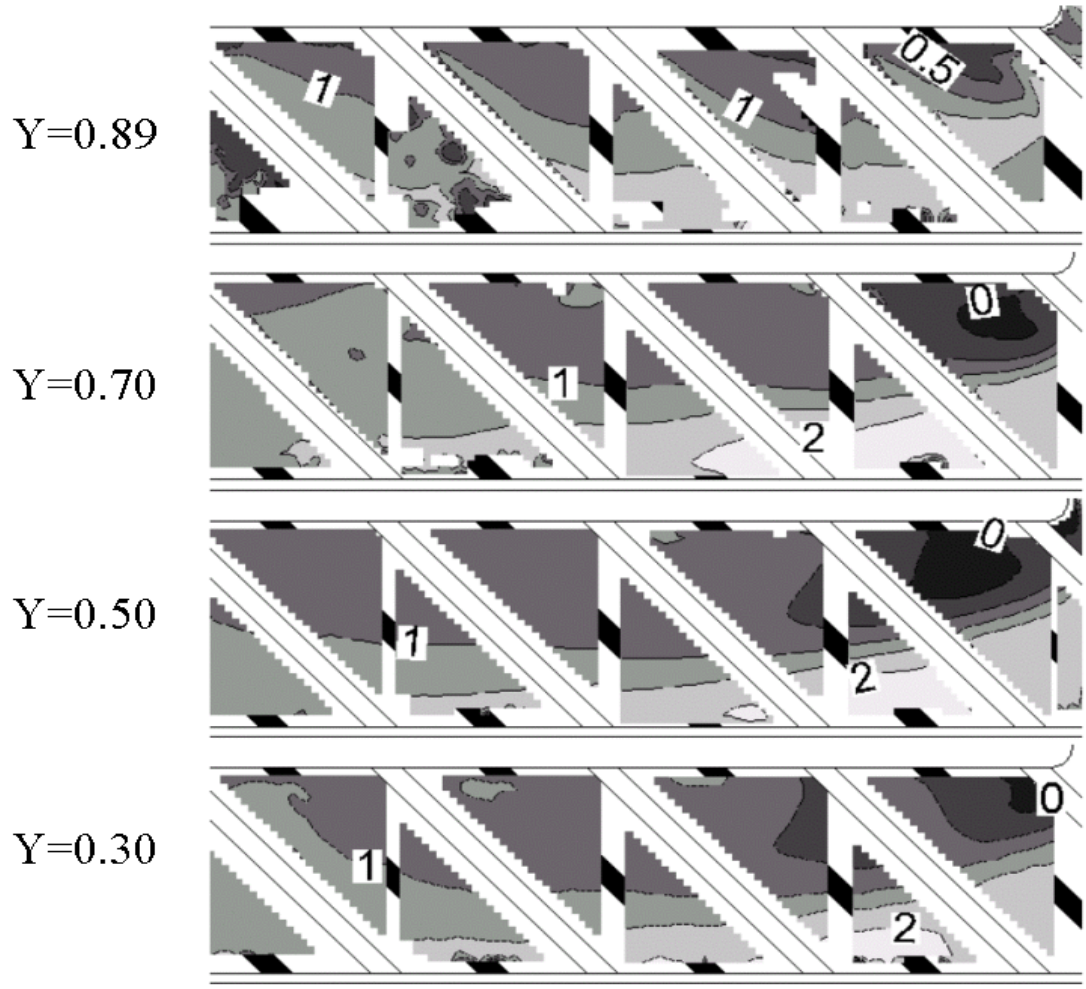

Figure 6: streamwise velocity contours immediately downstream of the bend, 0.0 < X < 4.0 at four distances from the bottom wall (U / Ub).

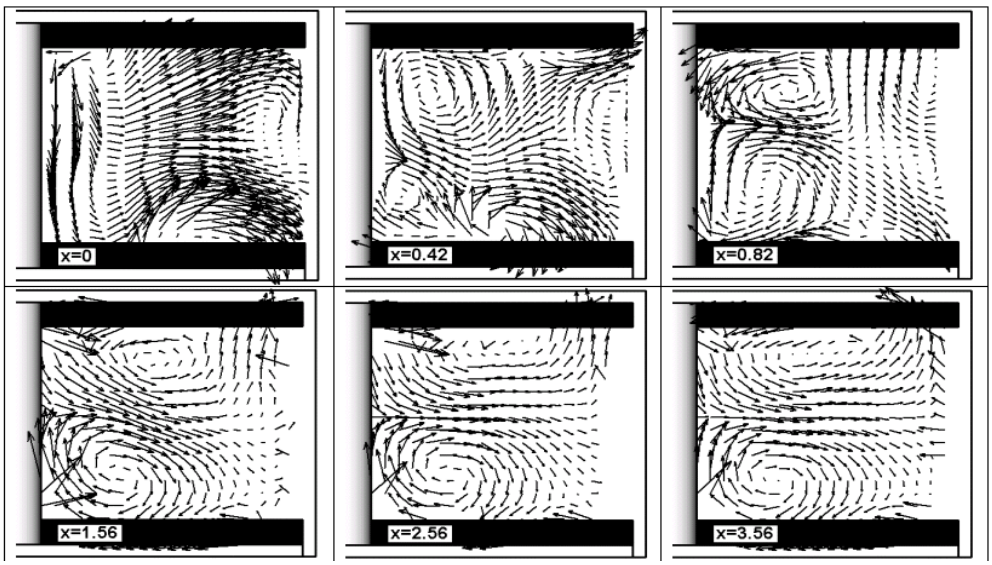

Figure 7: secondary flow vectors for 0.0 < X < 4.0. The plane locations are represented in Figure 2.

CONCLUSIONS

Three-dimensional velocity measurements were obtained in a two-legged blade coolant passage model with ribs orientated 45 deg to the passage. The model length, the rib locations and the geometry of the web between the coolant passage legs was more representative of gas turbine cooling designs than previously available geometries. The model employed is also the base geometry for a series of 4 configurations tested. The results from these measurements were compared with measurements in a similar model with a different web and rib arrangement.

Measurements in the developed flow region show details in the three velocity profiles that can be used to evaluate numerical simulation methods and turbulence or wall treatment models. The measurements showed the tendency of the streamwise and cross-stream velocities to be similar for various streamwise locations at the same cross-stream location.

Extending the ribs into the bend region and rounding the web at the entrance to the bend region decreased the size and length of the recirculation cell downstream of the bend, compared to previous geometries.

Extending the ribs into the bend region caused the recirculation zones in the outside corners of the bend to decrease, compared to previous geometries.

Separation of the flow from the end of the web end was delayed past 90 deg for the current geometry with the ratio of web thickness to passage width equal 0.2 and a full radius on the end of the web.

ACKNOWLEGDGEMENTS

This study was funded by the Swiss Office of Science in cooperation with the BriteEuram Internal Cooling of Turbine Blades project (contract number: BRPR-CT97-0600, project number: BE97-4022). The authors acknowledge the technical comments and editorial assistance of Dr. Bruce V. Johnson in the preparation of the paper.

REFERENCE

1. Lourenco, L.M., (1988). Some Comments on Particle Image Displacement Velocimetry. In: *Lecture Series* (Von Karman Institute for Fluid Dynamics), Vol. 06.
2. Schabacker, J. and Bölcs, A., (1996). *Investigation of Turbulent Flow by means of the PIV Method*. Proceedings of the 13th Symposium on Measuring Techniques for Transonic and Supersonic Flows in Cascades and Turbomachines. Zurich, Switzerland. 1996.
3. Prasad, A.K. and Adrian, R.J. (1993). Stereoscopic Particle Image Velocimetry Applied to Liquid Flows. *Experiments in Fluids*, 15 , 49-60.
4. Westerweel, J. and Nieuwstadt, F.T., (1991). Performance Tests on 3-Dimensional Velocity Measurements with a Two-Camera Digital Particle-Image-Velocimeter. In: *Laser Anemometry*), Vol. 1, 349-355.
5. Schabacker, J., Bölcs, A. and Johnson, B.V., (1998). *PIV investigation of the flow characteristics in an internal coolant passage with two ducts connected by a sharp 180° bend.* Proceedings of the International Gas Turbine & Aeroengine Congress & Exhibition. Stockholm, Sweden. 1998. ,98-GT-544.
6. Schabacker, J., (1998). PIV investigation of the flow characteristics in an internal coolant passages of gas turbine airfoils with two ducts connected by a sharp 180° bend. In: *Thesis* (Ecole Polytechnique fédérale de Lausanne), Vol. n°1816.
7. Raffel, M., Willert, C.E. and Kompenhans, J., (1997). Particle Image Velocimetry. A practicle guide.(Springer), ISBN 3-540-63683-8.
8. Bendat, J.S. and Piersol, A.G., (1986). Random data. In: *Random data* (John Wiley & Sons, Inc.), pp 82-86.
9. Bohnof, B., Schabacker, J., Parneix, S., Leusch, J., Johnson, B.V. and Bölcs, A., (1998). *Experimental and numerical study of developed flow and heat transfer in*

coolant channels with 45 and 90 degree ribs. Proceedings of the Turbulent heat transfer II. Manchester, UK. 1998. 99-GT-123.

10. Schabacker, J., Bölcs, A. and Johnson, B.V., (1999). *PIV investigation of the flow characteristics in an internal coolant passage with 45° rib arrangement.* Proceedings of the International Gas Turbine & Aeroengine Congress & Exhibition. Indianapolis, Indiana, USA. 1999. 99-GT-120.